THE JOURNAL OF PHYSICAL CHEMISTRY C

Article

pubs.acs.org/JPCC

Atomic Insight into the Layered/Spinel Phase Transformation in Charged $LiNi_{0.80}Co_{0.15}Al_{0.05}O_2$ Cathode Particles

Hanlei Zhang,[†,‡,§] Khim Karki,[‡,∥,§] Yiqing Huang,[‡] M. Stanley Whittingham,[‡] Eric A. Stach,[∥] and Guangwen Zhou*[,†,‡]

[†]Materials Science and Engineering Program and Mechanical Department and [‡]NorthEast Center for Chemical Energy Storage, State University of New York, Binghamton, New York 13902, United States

[∥]Center for Functional Nanomaterials, Brookhaven National Laboratory, Upton, New York 11973, United States

Supporting Information

ABSTRACT: Layered $LiNi_{0.80}Co_{0.15}Al_{0.05}O_2$ (NCA) holds great promise as a potential cathode material for high energy density lithium ion batteries. However, its high capacity is heavily dependent on the stability of its layered structure, which suffers from a severe structure degradation resulting from a not fully understood layered → spinel phase transformation. Using high-resolution transmission electron microscopy and electron diffraction, we probe the atomic structure evolution induced by the layered → spinel phase transformation in the NCA cathode. We show that the phase transformation results in the development of a particle structure with the formation of complete spinel, spinel domains, and intermediate spinel from the surface to the subsurface region. The lattice planes of the complete and intermediate spinel phases are highly interwoven in the subsurface region. The layered → spinel transformation occurs via the migration of transition metal (TM) atoms from the TM layer into the lithium layer. Incomplete migration leads to the formation of the intermediate spinel phase, which is featured by tetrahedral occupancy of TM cations in the lithium layer. The crystallographic structure of the intermediate spinel is discussed and verified by the simulation of electron diffraction patterns.

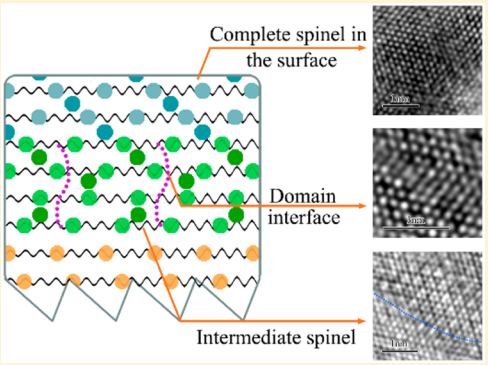

INTRODUCTION

Layered $LiNi_{0.80}Co_{0.15}Al_{0.05}O_2$ (NCA) is a promising cathode material for lithium ion batteries (LIBs), which has a high rate capability, a long lifetime, and theoretically a high specific capacity.[1−4] In NCA, 5% of aluminum substitutes for the TM cation sites, and the added aluminum remains as Al^{3+}. Al^{3+} is electrochemically inactive and cannot participate in the redox transformation, which has the beneficial effect of improving the structural stability and preventing the material from over-charge.[2] Thus, the NCA layered structure can undergo longer term cycling without collapsing into an inactive rock-salt phase. However, NCA suffers from another structural degradation mode. The layered → spinel phase transformation easily occurs[5−7] and irreversibly changes the surface region from the $R\bar{3}m$ structure to the $Fd\bar{3}m$ structure.[8−10] The spinel phase formed in the surface region increases the impedance of NCA,[11,12] reduces the electrochemical activity,[13,14] and diminishes the overall capacity.[15,16] Once the spinel phase forms, it can further decompose into a rock-salt phase,[17,18] which has an even higher impedance and further decreases the electrochemical performance.

The layered → spinel phase transformation occurs via the migration and rearrangement of TM atoms within the same oxygen framework.[19,20] In the pristine layered structure, oxygen ions are close packed in an O3 form, which provides the frame of the structure,[21] and TM/Li ions are inserted into the octahedral sites of the close-packing oxygen anions.[22] The lithium ions lie between slabs of octahedrons formed by the TM and oxygen, forming a layered structure. During the phase transformation, 1/4 of the TM cations shift into the lithium layers, which results in the formation of a cubic spinel structure.[18,22] The special chemical composition of NCA makes its phase transformation very different from other layered dioxides:[3] the Al^{3+} ions in NCA are highly movable and easily travel into the lithium layer,[16−18] which prohibits the whole structure from collapsing into a rock-salt phase.[23] However, this also accelerates the spinel transformation. Al^{3+} is known to stabilize the spinel structure,[1,24,25] which leads to the formation of a considerable amount of the spinel/intermediate spinel phases during the electrochemical reaction. The spinel phase is featured by the migration of TM cations from the 3a sites of the layered phase onto the 4d sites of the spinel phase,[26] which takes 5 steps.[20] The intermediate spinel is featured by incompletion of the 5 steps.[27] Regardless what the specific layered dioxide is, the structure of the intermediate spinel has long been an unsettled problem. Density functional theory (DFT) calculation by Ceder etc.[6,12] has shown that the occupation of tetrahedral sites in the lithium layer is an

Received: October 10, 2016
Revised: January 10, 2017
Published: January 11, 2017

DOI: 10.1021/acs.jpcc.6b10220
J. Phys. Chem. C 2017, 121, 1421−1430

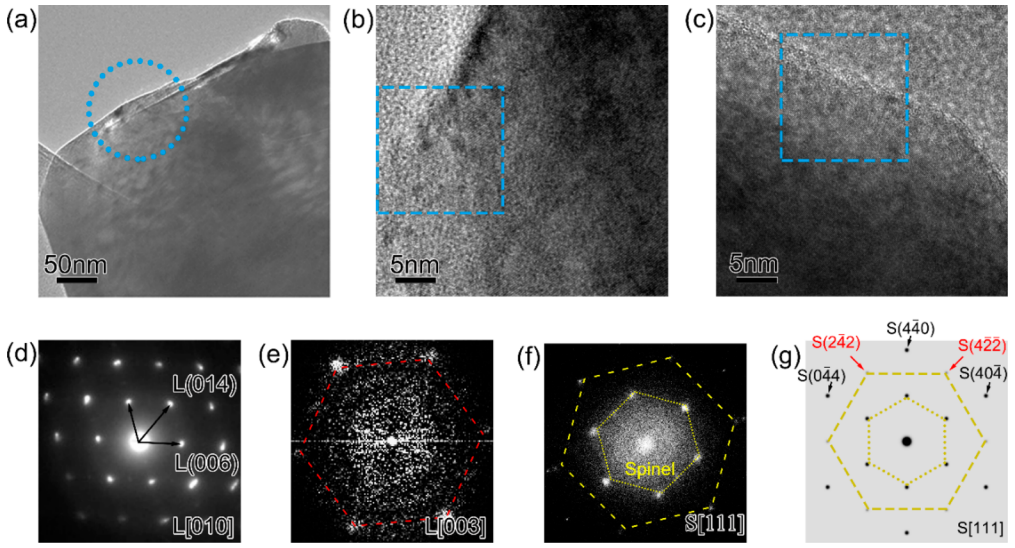

Figure 1. (a) TEM image of the pristine NCA particle. (b, c) HRTEM images of the NCA particle charged to 4.7 V ($Li_xNi_{0.8}Co_{0.15}Al_{0.05}O_2$, $x = 0.1$). (d) SAED pattern of the selected region in a, where the layered spots are indexed. (e) Diffractogram of the selected region in b, where the layered spots are marked by the red hexagon. No spinel spot is observed in the diffractogram. (f) Diffractogram of the selected region in c, where the spinel spots are marked by the yellow hexagons. (g) Simulated electron diffraction pattern of the spinel phase from the [111] zone axis, with the important spots indexed. Labels "L" and "S" in d–g stand for the layered and spinel phases, respectively.

important feature of the intermediate spinel, which is more commonly known as the "dumbbell structure". By forming the intermediate spinel phase with tetrahedral occupancy, the energy barrier for the layered → spinel phase transformation is lowered, making the phase transformation easier to occur. In other words, the formation of the intermediate spinel phase with tetrahedral occupancy is an energetically favorable step for the layered → spinel phase transformation.

The tetrahedral occupancy has been indirectly proven by the observation of the layered → spinel phase transformation.[12,28] However, direct experimental evidence supporting the existence this structure is still lacking because of the difficulty of capturing the intermediate spinel and obtaining atomic resolution data. In this study, industry-level NCA is used to extract the information relevant to a real battery. While the formation of the intermediates spinel is an energetically inevitable step for the layered → spinel phase transformation,[6] the intermediate spinel is very difficult to capture because it decomposes rapidly into the complete spinel. Even if the intermediate spinel can persist to some level during cycling, the TEM image contrast from the intermediate spinel can be convoluted with other defects that form during the cycling process. Therefore, we chose the sample that was charged to 4.7 eV to drive the formation of the intermediate spinel.[29,30] Without further cycling the sample, the intermediate spinel still does not completely transform to the complete spinel phase and there is a sufficient amount of the intermediate spine that can be captured by TEM. High-resolution transmission electron microscopy (HRTEM) is used to observe the microstructure transformation at the atomic level, and fast Fourier transform (FFT)/electron diffraction is used to study the crystal structure transformation. On the basis of these, a crystal structure model for the intermediate spinel is proposed. The overall phase transformation mechanism is discussed and illustrated based on the TEM analysis.

METHODS

Sample Preparation. Pristine NCA material was obtained from TODA America Inc., with a nominated formula of $LiNi_{0.80}Co_{0.15}Al_{0.05}O_2$. The NCA material was prepared into cathode by mixing the active material, carbon black, and polyvinylidene fluoride (PVDF) with a weight ratio of 8:1:1 using the *N*-methyl-2-pyrrolidone solvent. The cathode with 3–5 mg of the active material was assembled in 2325-type coin cells in a glovebox filled with helium. The electrolyte was 1 M $LiPF_6$ dissolved in a mixture of ethylene carbonate (EC) and dimethyl carbonate (DMC), with a volume ratio of 1:1. The coin cells were cycled with a MPG2 multichannel potentiostat (Biologic). Galvanostatic cycling was performed at a rate of *C*/10 with a current density of 6 mA/g. The sample was charged to 4.7 V without discharging.

Transmission Electron Microscopy (TEM) Characterization. The TEM samples were prepared in a glovebox. The charged NCA was scraped from the electrode, dissolved in isopropyl alcohol (IPA), and sonicated for several minutes. Finally, the dispersed solution was drop cast on TEM copper grids coated with a carbon film. The TEM observation was performed using an FEI Titan 80-300 microscope equipped with a field emission gun (FEG) and an aberration corrector (tuned to approximately 20 mRad), operated at an acceleration voltage of 300 kV. All HRTEM imaging in our experiments was carefully controlled around the Scherzer defocus (2.9 nm for FEI Titan 80–300[31]) condition to achieve the optimum resolution of the image features. While the HRTEM image contrast depends on the imaging condition (e.g., defocus and specimen thickness), the periodicity feature of the HRTEM images does not change with the imaging condition.[32,33] Because the diffractogram of spots is determined by the periodicity feature of the HRTEM images, it can be employed for crystal structural fingerprinting. It has been shown that the e-beam irradiation can induce the phase transformation in the layered oxides for relatively long e-beam irradiation (>2 min)[34] or a high electron beam dose in a small area.[35] Beam effect is negligible for HRTEM or STEM imaging with a short beam

DOI: 10.1021/acs.jpcc.6b10220
J. Phys. Chem. C 2017, 121, 1421–1430

exposure.[26,36,37] In our experiments, the e-beam effect was carefully minimized by adjusting the imaging condition in one area and then moving to a neighboring, fresh area for HRTEM imaging. Additionally, no noticeable structure changes were observed by comparing a sequence of HRTEM images taken from the same area, further confirming the negligible e-beam effect in our experiments.

Structure Simulation. Simulation of the crystal structures and electron diffraction patterns was performed using CrystalMaker and SingleCrystal. Electron diffraction simulation was performed using the kinematic method with a specimen thickness of 50 Å and an intensity saturation of 10. The position information on diffraction spots in the simulated patterns is directly compared with that of the diffractograms of HRTEM images for structure determination. The lattice parameters of the layered and the spinel structures used for simulation were obtained from refs 38 and 39. In the layered structure ($R\bar{3}m$) TM atoms are located on 3a sites with Li atoms on 3b sites. For the spinel structure ($Fd\bar{3}m$), TM atoms are positioned on 16d sites with Li atoms on 8a sites.

RESULTS

Phase Transformation in Charged NCA. Figure 1 shows TEM/HRTEM images and corresponding electron diffraction patterns of NCA particles at the pristine state (Figure 1a and 1d) and after being charged to 4.7 V (Figure 1b, 1c, 1e, 1f, and 1g), where x = 0.1 in $Li_xNi_{0.8}Co_{0.15}Al_{0.05}O_2$). Our TEM observations show that there are no significant changes in the particle morphology and that the surface of the particles remains smooth after the charging process. The diffraction pattern of the pristine NCA (Figure 1d) shows that it has the typical layered structure without any detectable spinel phase. When charged to 0.1 Li, most areas still maintain the layered structure (Figure 1b and 1e), while in some surface areas (Figure 1c), a new structure forms in the surface region with a total thickness of 5−10 nm into the subsurface region. This structure is proven to be the spinel phase by the diffractogram (Figure 1f, where the spinel spots are marked with the yellow hexagons), which matches perfectly with the simulated diffraction pattern of the spinel structure as shown in Figure 1g. This demonstrates that the layered phase has decomposed into the spinel structure in some surface regions during the charging process, which can lead to a diminished electrochemical performance.

Microstructure Evolution. Figure 2a is an HRTEM micrograph showing the surface area of the sample charged to 4.7 V ($Li_xNi_{0.8}Co_{0.15}Al_{0.05}O_2$, x = 0.1), and Figure 2b is an overall diffractogram of Figure 2a. The yellow hexagons correspond to the spinel spots, as marked. An unknown diffractogram is present as indicated by the red lines, which does not belong to either the spinel or the layered phase. For now, it is referred as "unknown structure", as will be explained later.

From previous work,[5,14] it is evident that the layered → spinel transformation occurs first in the surface region of the particle and then propagates toward the interior of the particle. Different microstructures may develop as the transformation propagates inward. Considering this, three representative areas, as marked by A, B, and C in Figure 2a, have been selected from the very surface to the subsurface region for detailed analysis.

Figure 3 shows a magnified HRTEM micrograph from the surface region of the charged particle (i.e., region A in Figure 2a) and its corresponding diffractogram, where all spinel spots

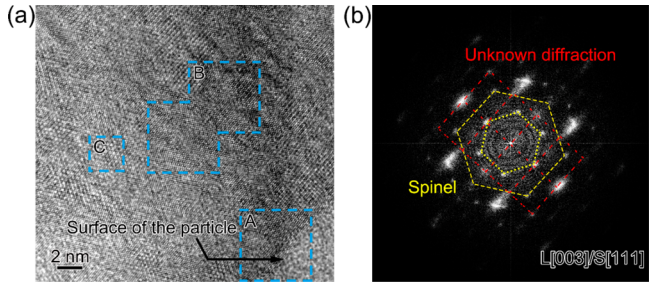

Figure 2. Sample charged to 4.7 V (x = 0.1 in $Li_xNi_{0.8}Co_{0.15}Al_{0.05}O_2$). (a) HRTEM image from the surface region of the particle. Three areas, A, B, and C, are selected for detailed analysis shown later. (b) Overall diffractogram of a, where the spots associated with the spinel phase are marked by the yellow hexagons and the red lines correspond to the unknown structure.

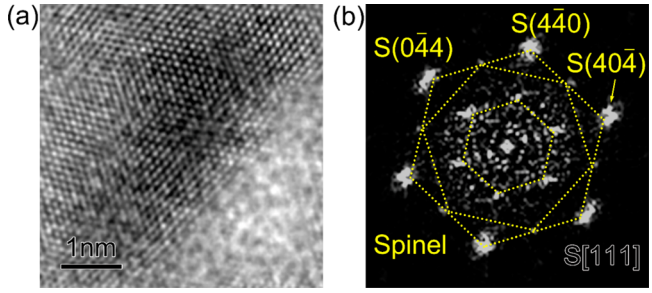

Figure 3. (a) HRTEM image from the surface region of the charged particle. (b) Diffractogram of the HRTEM image in a, indicating that the surface region is completely transformed to the spinel phase.

are present, as marked by the yellow hexagons (Figure 3b). There are no spots associated with the layered structure, i.e., the layered phase is completely transformed into the spinel phase in the surface region.

Figure 3a shows that the spinel phase has a relatively intact lattice structure with almost no internal defects or interfaces. This can be attributed to the complete topotactic transformation (layered → spinel):[40−42] the transformation occurs via gradual migration of TM atoms from the TM layer into the Li layer. Because the two phases are highly compatible, there are no obvious interfaces or significant lattice distortion occurring during the layered → spinel phase transformation. Also, the lattice parameters change very little, which causes negligible internal strain, as evidenced by the absence of extended structural defects such as dislocations or stacking faults in the surface region.

Figure 4a shows a magnified HRTEM image of region B marked in Figure 2a, which is about 10 nm away from the outermost surface of the particle. Figure 4b is the diffractogram of the HRTEM image in Figure 4a, which indicates that this region is dominated by the spinel phase (the spinel spots are marked out with yellow hexagons). Figure 4a shows that stripe-shaped spinel domains have formed in this region and the spinel stripes are elongated along the $[02\bar{2}]_S$ direction with a finite thickness (~0.5 nm) of the domain boundaries. The formation of these high-density spinel domains suggests that the layered → spinel transformation occurs via a nucleation and growth process, in which the nucleated spinel domains grow preferentially along the $[02\bar{2}]_S$ direction, resulting in the stripe morphology. These stripe-shaped domains merge laterally to form $(4\bar{2}\bar{2})_S$-type domain boundaries. In Figure 4a, the domain interface region is highly coherent with the spinel domains on

DOI: 10.1021/acs.jpcc.6b10220
J. Phys. Chem. C 2017, 121, 1421−1430

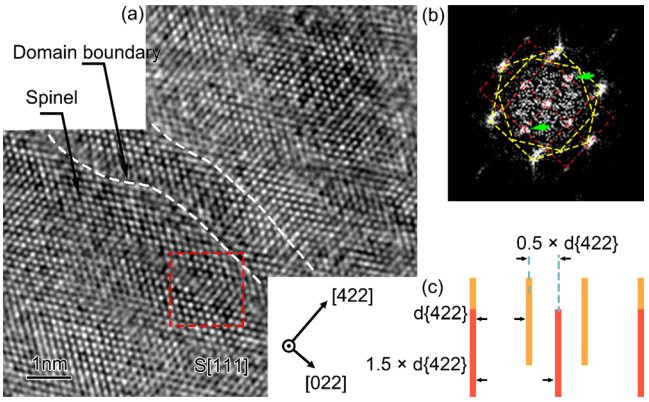

Figure 4. (a) HRTEM image from the subsurface region (~10 nm deep from the outermost surface region), showing the formation of stripe-shaped spinel domains with the domain boundaries of a finite thickness, as marked out by the dashed white lines. (b) Diffractogram of the HRTEM image of a, showing the presence of the intrinsic spinel spots marked out by yellow hexagons and the unknown diffraction spots marked out by red lines. (c) Schematic showing the interweaved atomic planes of the complete and intermediate spine phases, where the yellow and red lines refer to the atomic planes of the complete and intermediate spine phases, respectively.

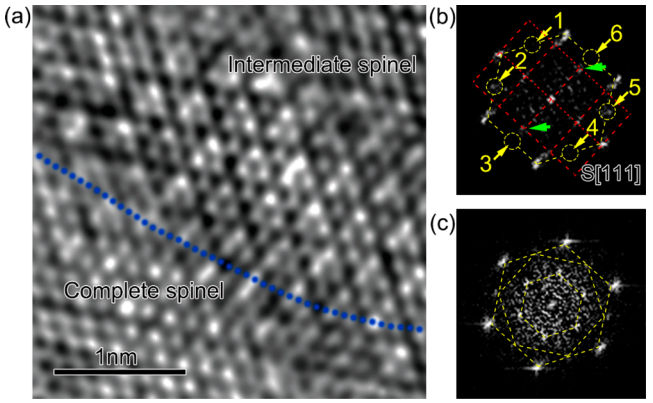

Figure 5. (a) HRTEM image of region C in Figure 2a. The complete spinel phase and the intermediate spinel phase form in different regions, with their interface marked out by a blue dashed line. (b) Diffractogram from the upper-right region of a. Yellow hexagon and yellow dashed rings mark out the intrinsic spinel spots, and red lines mark out the unknown diffraction. Numbered yellow rings mark out the possible {422} spinel spots, among which only the no. 2 and 5 spots can be observed, while the rest are weak or missing. (c) Diffractogram from the lower-left region of a. Yellow hexagons mark out the spinel spots.

both sides. Because these spinel domains are all transformed from a single particle of the layered phase via the nucleation and growth process, the domains inherit the crystallographic orientation of the parent layered grain and are therefore aligned well. The domain boundary areas show a slightly disrupted lattice structure because of small misorientations between domains. As seen from the diffractogram shown in Figure 4b, the unknown diffraction (indicated by red lines), which are the same as those in the diffractogram of Figure 2b, are present again. The spinel nature of region B is evident according to the featured spots (marked by yellow hexagons), but the {220}-type intrinsic spots are missing: an unknown diffraction pattern forms instead. This suggests that the spinel structure is incomplete, or better termed as the "intermediate spinel". As shown in Figure 4a and 4b, the intermediate spinel phase forms as nanometer-size domains with its lattice planes interweaved with the complete spine phase and the two phases do not show clear phase separation, as illustrated schematically in Figure 4c. The interweaving of the atomic planes of the complete and intermediate spinel phases makes them indistinguishable in the HRTEM images. Without HRTEM images showing the intermediate phase only, it is impossible to use HRTEM image simulation to determine the crystal structure. Instead, a diffractogram is capable of resolving in the reciprocal space the difference in the periodicity of the atomic planes of the two phases and is therefore employed for structure determination in the Discussion section. It is also worth mentioning that the stripe-shaped domains shown in Figure 4 have a curved morphology with random spacings between domains, which is very different from the image contrast of Moiré fringes that are parallel and periodic as a result of interference between diffracted beams from overlapping lattices. This is also confirmed from the diffractograms shown in Figures 2, 4, and 5, which do not show the presence of satellite spots around the basic reflections. The lack of Moiré fringes and double diffraction is because of the interweaved lattice planes of the two phases, for which there is no strict overlapping of the lattices of the complete and intermediate spine phases.

Figure 5a shows an HRTEM image from another representative subsurface region (i.e., region C in Figure 2a, which is ~15 nm deep from the surface). Figure 5b is the diffractogram from the upper-right region of Figure 5a (the spinel spots are marked with a yellow hexagon and yellow rings). This diffractogram is very similar to the diffractograms in Figure 4b: the featured spinel spots are only partially present, and an unknown diffraction occurs, suggesting that the spinel phase is also an "intermediate spinel" phase. There are even fewer intrinsic spinel spots in Figure 5b compared with Figure 4b: for the {442}-type spots (marked with yellow rings), only nos. 2 and 5 are evident. nos. 1 and 4 are only weakly present, and nos. 3 and 6 are entirely missing. This suggests that region C has even less spinel character and is closer to the intermediate spinel. The intermediate spinel can be considered similar to the spinel phase reported by Guilmard[23] and Ryoo[19] in charged $LiNi_{0.70}Co_{0.15}Al_{0.15}O_2$ and $LiMn_{1.5}Ni_{0.5}O_4$ annealed at 700 °C. The structure of the intermediate spinel will be discussed later in the Discussion section. Figure 5c is the diffractogram from the lower-left region of Figure 5a, showing this region is the complete spinel phase. An interface can be observed between the intermediate spinel and the complete spinel, suggesting that the layered phase is first transformed to the intermediate spinel and subsequently transformed into the complete spinel.

As can be seen from Figure 5a, the lower-left-corner region corresponds to the completely transformed spinel phase, which shows a close-packing lattice structure with a relatively uniform image contrast. The upper-right region is the intermediate spinel phase with a less close-packing structure, where the TM migration is incomplete and the 4d sites are not fully occupied by TM atoms, thereby reducing the packing efficiency. The missing 4d atoms make the appearance of the lattice structure in the intermediate spinel phase region very different from the regions that have been completely transformed to the spinel structure.

DOI: 10.1021/acs.jpcc.6b10220
J. Phys. Chem. C 2017, 121, 1421−1430

DISCUSSION

Structure Transformation during the Layered → Spinel Phase Transformation. The diffractograms of the surface and subsurface regions (i.e., regions A−C (Figures 3−5)) indicate that the surface region of the charged NCA particle is completely transformed to the spinel phase and the subsurface is dominated by an intermediate spinel phase with an unknown structure. To solve the unknown structure of the intermediate spinel phase, both the mechanism of its formation and the resulting diffractions have to be considered.

In the process of electron diffraction, the contribution of lithium ions to the diffraction pattern is minimal because the atomic-scattering factor of lithium is very low,[43] especially when there is only 10% of lithium in the NCA charged to 4.7 V. Meanwhile, the oxygen frame does not change during the phase transformation; thus, the oxygen anion positions do not affect the diffraction pattern. Therefore, only the locations of TM atoms should be considered when analyzing the unknown diffraction pattern.

The diffractogram features of the intermediate spinel can be described as follows: the $\{220\}_S$-type spinel spots are missing, while a set of unknown diffraction spots is generated. During the layered → spinel phase transformation, 1/4 of the TM cations travel from the TM layers into the neighboring lithium layers and settle on the 4d sites; 3/4 of the TM cations remain in the TM layers and reside at the 12d sites.[44] The 12d TM cations maintain the layered characteristics, which contribute to the $\{440\}_S$-type spots. The 4d sites represent the cubic feature of the spinel, and the occupation of these sites by the TM atoms generates the $\{220\}_S$-type spots.[45] Therefore, the absence of {220} spots is due to the incomplete occupancy of the 4d sites.

Guilmard et al.[20,46] proposed a 5-step migration path for TM atoms from the 3a layered site onto the 4d spinel site, namely, TM_{oct} (A) → TM_{tet} (B) → TM_{oct} (C) → TM_{tet} (D) → TM_{oct} (E), as shown in Figure 6a. In the first step (TM_{oct} → TM_{tet}, site A to B) TM atoms migrate from the TM layer into the lithium layer. In the following steps, the TM atoms only move within the lithium layer. If the five steps are not fully fulfilled, TM atoms will stay on an intermediate site. The incomplete migration of the TM atoms leads to the formation of an intermediate spinel, which is the reason for the missing of {220}-type spots and the formation of the unknown diffraction pattern. In the unknown diffraction pattern (Figures 4b and 5b), the two spots marked with green arrows are along the $[4\bar{2}\bar{2}]_S$ direction. In Figure 6a, sites B and C are along the ⟨422⟩ direction of the spinel structure. If TM atoms stay on these two sites, the structure factors for planes perpendicular to ⟨422⟩ will be different from the complete spinel phase. This can lead to the formation of the unknown diffraction spots in Figures 4b and 5b, which are associated with the atomic planes perpendicular to the ⟨422⟩ direction.

Figure 6b shows a [111] projection view of the spinel structure, where the filled blue circles represent TM atoms. The $\{4\bar{2}\bar{2}\}$ planes are marked with black broken lines. As discussed in the last paragraph, the atomic planes parallel to $(4\bar{2}\bar{2})$ are changed if sites B and C are taken by TM atoms. It can be identified from the diffractograms shown in Figures 4b and 5b that the marked spots (green arrows) have a diffraction vector of $|\mathbf{g}_u| = \frac{2}{3}|\mathbf{g}_{\{4\bar{2}\bar{2}\}}|$, which corresponds to 1.5 times the lattice spacing of $(4\bar{2}\bar{2})$. In the complete spinel structure, such crystal planes with thae lattice spacing of 1.5 times $(4\bar{2}\bar{2})$ have the

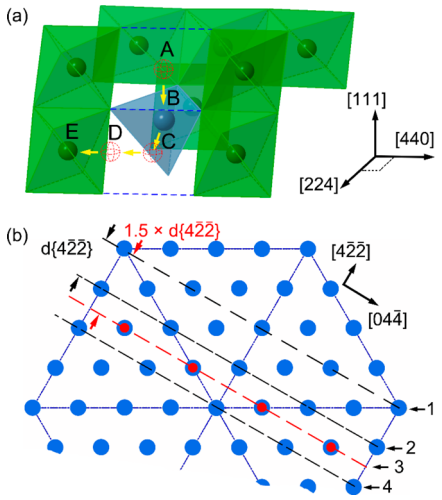

Figure 6. (a) Schematic illustration of the migration path of TM atoms from the 3a sites (layered) onto the 4d sites (spinel) via a path of A → B → C → D → E, where A corresponds to the layered 3a site and B, C, D, and E correspond to the tetrahedral and octahedral sites in the lithium layer. B is the 8a site of the spinel phase, and E is the 4d site of the spinel phase. The incomplete migration of TM atoms results in the formation of the intermediate spinel structures. (b) [111] projection view of the spinel structure. Blue circles represent TM atoms in the complete spinel structure, and red circles represent TM atoms on B (8a) sites. Red/black broken lines correspond to the atomic planes parallel to the $(4\bar{2}\bar{2})$ planes, which are marked 1−4.

value of the structure factor to be zero and are thus systematically absent. The diffraction factor can be transformed by positioning TM atoms on the 8a site (namely, the B site in Figure 6a), as shown with the red circles (Figure 6b). By doing this, a new plane is generated (i.e., line 3, marked by the red broken line shown in Figure 6b). The spacing between line 1 (the atomic plane associated with the complete spinel structure) and line 3 (the new plane formed by placing TM atoms on 8a) is 1.5 times $d\{4\bar{2}\bar{2}\}$, which is consistent with the diffraction spots with the diffraction vector of $|\mathbf{g}_u| = \frac{2}{3}|\mathbf{g}_{\{4\bar{2}\bar{2}\}}|$.

As shown in Figure 6a, TM atoms staying on the C site (octahedral) can also change the atomic planes perpendicular to $[4\bar{2}\bar{2}]_S$. However, the C site is too close to the 4d spinel site. The strong repulsive force between C-site cations and 4d cations makes the occupancy of the C site by TM atoms energetically unfavorable.[47] As seen from Figure 6a, the B site actually belongs to the 8a site of the spinel structure and should be originally occupied by Li^+ for a complete spinel structure,[18] so the occupancy of the 8a site with TM cations is energetically allowed. The occupancy of this site by TM atoms changes the structure of the spinel phase, which can be considered as an intermediate spinel phase. TM atoms on the 8a sites block the diffusion channels for Li^+ cations, which can therefore impede the transportation of Li cations and thus hamper the electrochemical performance. The effect from the formation of the intermediate spinel phase can be similar to the blocking effect associated with the formation of the rock-salt structure. Even if the blocking happens just at one site, it can hold up the entire diffusion channel and significantly reduce the Li^+ ion conductivity.

We use electron diffraction simulation to more precisely determine the structure of the intermediate spinel phase described above. Figure 7a is the reciprocal lattice of the intermediate spinel phase extracted from the unknown

DOI: 10.1021/acs.jpcc.6b10220
J. Phys. Chem. C 2017, 121, 1421−1430

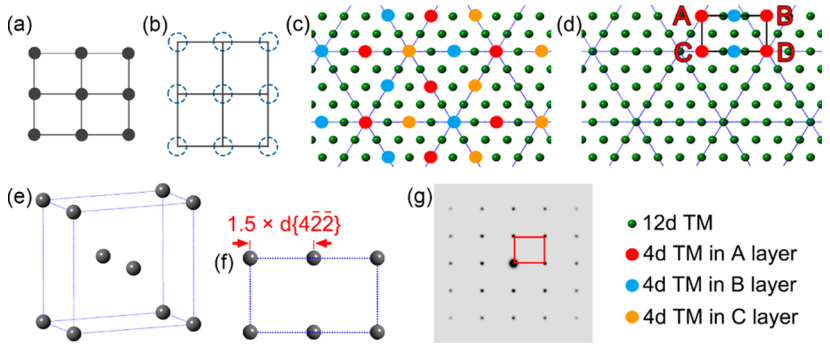

Figure 7. (a) Reciprocal lattice of the intermediate spinel extracted from the unknown diffraction in Figures 4b and 5b. (b) Corresponding [111] projection view of the real lattice of the intermediate spinel phase. (c) [111] projection view of the complete spinel structure. Green circles represent 12d TM cations, and red/blue/yellow circles represent 4d TM cations in A/B/C layers, respectively. (d) Possible crystal structure based on the reciprocal lattice of the intermediate spinel in a. (e) 3D view of the proposed structure. (f) [111] projection view of the proposed structure. (g) Simulated [111] diffraction pattern of the proposed structure.

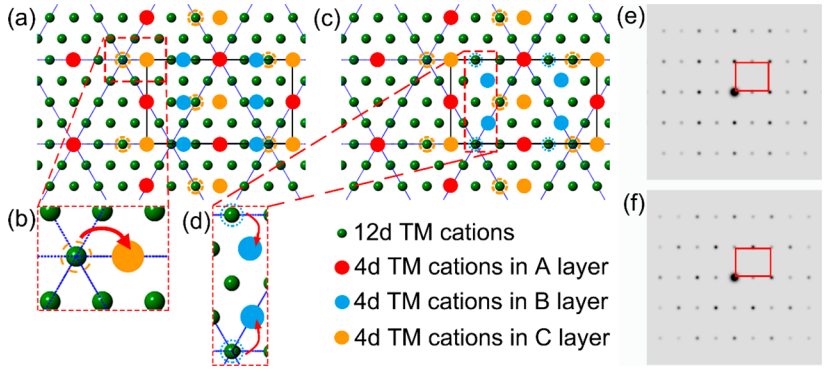

Figure 8. (a, c) Two modified crystal structures based on the first structure of the intermediate spinel in Figure 7. (b and d) Enlargements of the selected areas in a and c, showing the featured migration of 4d TM cations. (e and f) [111] diffraction patterns of the two proposed structures.

diffraction pattern shown in Figures 4b and 5b. Figure 7b is the corresponding [111] projection view of the real lattice of the intermediate spinel phase. Figure 7c shows a [111] projection view of the complete spinel structure. The 12d TM cations are represented with green circles. Because the oxygen frame has an FCC structure, the 4d TM cations exhibit an ABCABC stacking sequence, as represented by the larger red/blue/yellow circles in Figure 7c, respectively. Li and O ions are not shown since they do not contribute to any changes in the diffraction patterns. As discussed in Figure 6, the incomplete migration onto 4d sites leads to the formation of the intermediate spinel structure. Therefore, the 4d sites (red/blue/yellow circles in Figure 7c) of the intermediate spinel should not be fully occupied, and some other sites (which are not occupied in the complete spinel) in the lithium layer should be occupied by TM cations, making the atomic configuration of the intermediate spinel different from the complete spinel shown in Figure 7c.

Figure 7d is a possible configuration of the intermediate spinel derived from the reciprocal lattice shown in Figure 7a. In this structure, A and D cations are the original 4d cations in the A layer of the complete spinel, which remains unchanged in the intermediate spinel. B and C cations are also in the A layer but migrated from elsewhere to their current sites. The two blue cations are originally 4d cations in the B layer of the complete spinel, transferred from the original sites onto the new sites in Figure 7d (still in B layer). The "C layer" of the intermediate spinel is the same as the A layer, so the structure has an ABAB... stacking sequence. As seen in its 3-D view (Figure 7e), it is a bottom-centered structure. The CIF file of this structure can be found in the Supporting Information.

The simulated [111] diffraction pattern from the proposed structure (Figure 7g) matches the actual diffraction patterns (Figures 4b and 5b) very well. The [111] projection view (Figure 7f) of the structure indicates a d spacing of 1.5 times $d\{4\bar{2}\bar{2}\}$, which is the key feature to form the unknown diffraction pattern (especially the two spots marked by green arrows in Figures 4b and 5b). However, this structure is purely derived by the diffraction pattern, and the diffraction pattern is an average description of the crystal structure. Therefore, the proposed structure (Figure 7d) is also an average description of the intermediate spinel phase. The local occupancy of TM cations can deviate from this structure (in this case, by "local" we refer to atomic level). An obvious "average feature" associated with this structure is that the two B-layer atoms are located on neither octahedral nor tetrahedral sites of the O frame (Figure 7d), making this structure less energetically stable. A second sign of averaging is related to presence of the B and C cations in the A layer, as shown in Figure 7d. These two cations are extra cations, so they have to migrate from elsewhere to the new sites in Figure 7d, which may be an energetically costly process. Therefore, the siting of TM cations in local regions should be different from the "average structure" proposed in Figure 7d, which we discuss below.

Figure 8a is another possible configuration of the intermediate spinel. Compared to the complete spinel, the A layer remains unchanged and the entire C layer migrates synchronously onto the adjacent tetrahedral sites, as shown in

DOI: 10.1021/acs.jpcc.6b10220
J. Phys. Chem. C 2017, 121, 1421−1430

the zoom-in view (Figure 8b). The 4d cations in the B layer migrate from the 4d sites of the complete spinel onto the new sites in Figure 8a, which are the same as those in Figure 7d. This structure fixes the high-concentration-atom problem in the A layer, i.e., no extra cations are necessary in the A layer. The diffraction pattern of this structure (Figure 8e) is very close to that of the first structure but with some superstructure spots. This is because the unit cell of the second structure is 2 × 2 × 2 of the unit cell of the first structure (Figure 7d–f). A larger unit cell leads to a reduced reciprocal cell, as shown in Figure 8e. (The 3D model, [111] projection view, and CIF file of this structure can be found in the Supporting Information)

To improve the energetically unfavorable sitting of B-layer cations, a third structure model is proposed (Figure 8c and 8d). The A and C layers of this structure are the same as those of the second structure, while the B-layer cations are adjusted onto the tetrahedral sites. Figure 8d is a magnified view of the migration of B-layer TM cations from their original octahedral sites (4d) onto the neighboring tetrahedral sites. The diffraction pattern of the third structure (Figure 8f) has the same shape as that of the second structure (Figure 8e), but the relative intensities are different: some fundamental spots are weak, while some super structure spots are strong. This change is exclusively caused by changing the position of B-layer cations. (The 3D model, [111] projection view, and CIF file of this structure can be found in the Supporting Information).

As discussed above, the first structure is an overall, average structure model, which matches the experimental diffraction pattern well, but the B-layer cations are not on energetically favorable octahedral/tetrahedral sites. Also, it has too many cations in the A layer, which may cause lattice distortion and make the structure difficult to form. These two problems are resolved in the third structure, which is closer to the real local occupancy of TM cations and thus more energetically favorable. However, this structure exhibits extra superstructure spots which are not observed in the experimental diffraction patterns (Figure 4b and Figure 5b).

In the third structure, the superstructure spots arise from a 2 × 2 × 2 unit cell (compared to the first structure), and the sites of the B-layer cations affect the brightness of the diffraction spots. It is worth noticing that we propose the third structures assuming a highly ordered structure (Figure 8c). However, since the layered → spinel phase transformation is a random process and the intermediate spinel is metastable,[27] the intermediate spinel should be much less ordered. Thus, the lattice sites, those proposed in the third structure (Figure 8c), cannot be fully occupied. A random occupation of these lattice sites makes the average unit cell close to the first structure, which results in the diffraction pattern matching well with the experimental ones (Figures 4b and 5b). Therefore, the local TM occupation follows the mechanisms proposed in the third structure, but the lack of long-range ordering of the tetrahedral/octahedral occupation across multiple unit cells results in the averaged structure as shown in Figure 7d. In the third structure model, the B-layer and C-layer cations occupy tetrahedral sites in the lithium layer. This is consistent with our discussion in Figure 6b as well as the previous density functional theory (DFT) results,[6,12,48] which shows that the tetrahedral occupation is an energetically favorable mechanism to form the intermediate spinel.

Our structure models are built up by modifying the complete spinel phase, but the real transformation process should be intermediate spinel → complete spinel. The third possible structure can transform to the complete spinel by TM migration onto neighboring octahedral sites, without long-range migration in the lattice. Therefore, the tetrahedral occupation associated with this structure is an energetically and crystallographically favorable mechanism for the intermediate spinel.

Microstructure Evolution during the Phase Transformation. According to the HRTEM images shown in Figures 2–5, the microstructure of the particle varies from the surface to the subsurface region during the layered → spinel phase transformation. The surface region is completely transformed to the spinel phase. The subsurface region (~10 nm deep from the outermost surface) is dominated by stripe-shaped spinel domains and the intermediate spinel phase, along with a high density of domain boundaries. To have a better idea of the atomic structure in the domain boundary regions, Figure 9a presents a magnified HRTEM view of a representative

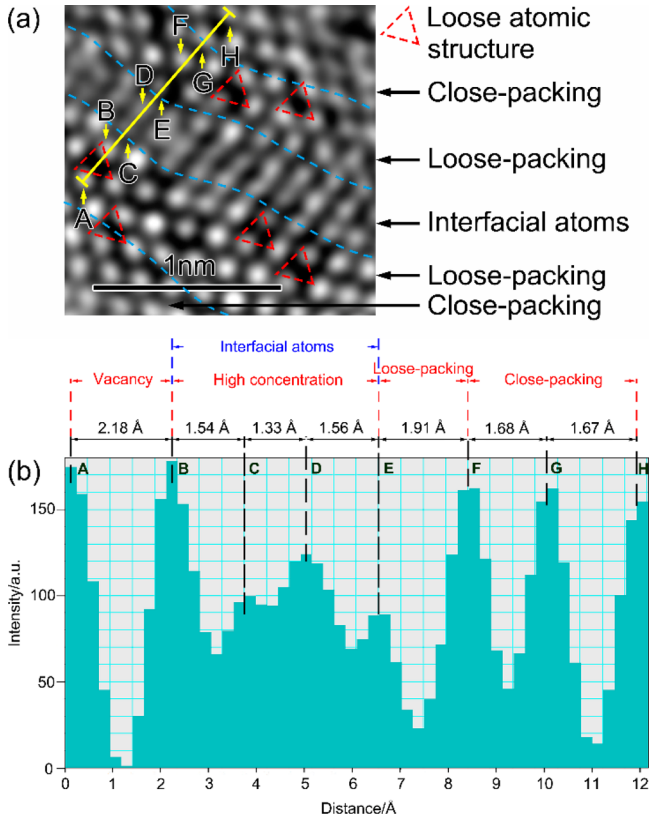

Figure 9. (a) Magnified HRTEM view of a representative domain boundary, namely, the region marked with a red square in Figure 4a. (b) Intensity profile across the domain boundary along the yellow line in a.

domain boundary, as marked by the dashed red square shown in Figure 4a. Figure 9b is an intensity profile obtained along the yellow line marked in Figure 9a. In Figure 9, the atomic columns across the yellow line are designated as A–H.

In the complete spinel, the distances between two adjacent atomic columns along the yellow line should be $d_{\{442\}}$, which equals 1.67 Å.[39] According to the intensity profile (Figure 9b), the distance between A and B is 2.18 Å, which is much larger than the $d_{\{442\}}$ for the complete spinel phase, suggesting the existence of a loose atomic structure (resembling voids) between A and B, as indicated in Figure 9a. Atomic columns B–E are within the domain boundary area and have smaller

DOI: 10.1021/acs.jpcc.6b10220
J. Phys. Chem. C 2017, 121, 1421–1430

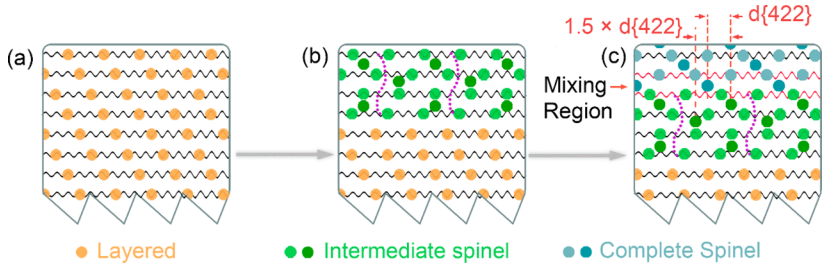

Figure 10. Schematic illustration of the microstructure evolution induced by the layered → spinel phase transformation within a single NCA particle. (a) Pristine particle of the layered phase. (b) Upon charging, spinel domains (intermediate spinel) form in the surface and the subsurface regions of the particle. (c) As the charging continues, complete spinel phase nucleates and grows within the intermediate spinel that results in complete spine in the surface and interwoven lattice planes of the two phases in the subsurface region. Mixing of the complete and the intermediate spinel forms on their interface. The domain boundary in the intermediate spinel phase is marked out with purple dashed lines.

interplanar spacings than that of the complete spinel structure (1.67 Å). This can be attributed to the high concentration of the TM atoms in the domain boundary region and thus smaller atomic spacings in the projection view of the domain boundary area. The distance between E and F is 1.91 Å, which is larger than $d_{\{442\}}$. For atomic columns F−H, the interplanar spacings are 1.67 Å, which is very close to the $d_{\{442\}}$ of the complete spinel structure.

Therefore, a higher density of atomic columns can develop within the domain boundary region (the interfacial atoms in Figure 9, atomic columns between B and E). The atom columns next to the domain walls are loose packing (e.g., the spacing between A and B and the spacing between E and F), and there is a restoration of close packing in the region about two atomic spacings away from the domain boundary. The HRTEM images were obtained under the Scherzer defocus condition, for which the bright contrast of atom columns can be obtained bright.[49,50] In addition to the instrument setup, the HRTEM image contrast also depends on the thickness of the specimen. The dark columns as marked by red dashed triangles in Figure 9a are not necessarily complete vacancy columns. Instead, they can be vacancy-containing atom columns (i.e., with loose atomic packing along these columns)

Adjacent to the high-concentration domain wall is the loose-packing region. This is a sudden transformation from the high concentration to a low concentration, without an intermediate region. Accordingly, the high concentration of TM atoms on the domain boundary migrates from neighboring loose-packing areas. The intermediate spinel nucleates on the domain boundary, and loose atomic structures form adjacent to the domain boundary, as shown in Figure 9. Since the intermediate spinel nucleates on the domain boundary area, its projection view (Figure 9a) presents an overly close-packed structure.

Figure 10 schematically summarizes the microstructure evolution induced by the layered → spinel phase transformation within a single NCA particle during the charging process. The pristine particle (Figure 10a) can be viewed as a single crystal with the layered structure. Upon charging (Figure 10b), spinel domains (the intermediate spinel) form in the surface region of the particle and then grow inward. As discussed above, the layered → spinel transformation occurs by a topotactic reaction via random nucleation of spinel domains in the parent particle of the layered phase, so the newly formed spinel domains are highly coherent with the parent layered phase. As the charging continues (Figure 10c), the spinel domains merge, resulting in a spinel shell in the surface region. The complete spinel/intermediate spinel boundary is a mixing of the two phases. In the subsurface region, the spinel domains do not merge completely, resulting in domain boundaries with a finite thickness of ~0.5 nm. The spinel domains develop into a stripe-shaped morphology by growing preferentially along the $[0\bar{4}4]_S$ direction (Figure 10c). The incomplete migration of TM atoms results in the formation of an intermediate spinel phase in the subsurface region.

CONCLUSION

We performed a detailed TEM investigation of NCA cathode particles charged to 4.7 V and observed a core−shell structure induced by the layered → spinel phase transformation. Spinel phase forms in the surface region of NCA particles during charging and propagates inward toward the core area. A complete spinel structure forms in the near surface area, and spinel domains and intermediate spinel are present deeper in the subsurface region. The layered → spinel phase transformation occurs via migration of TM atoms, from the 3a layered sites onto the 4d spinel sites. The migration occurs via a 5-step pathway, and incomplete migration of the TM atoms leads to the formation of an intermediate spinel with an interplanar spacing of $\frac{3}{2}d\{4\bar{2}2\}$, an observation supported by electron diffraction. On the basis of the structural information from HRTEM and diffractogram as well as the considerations of reducing the total free energy, a possible structure of the intermediate spinel is proposed, which suggests that the TM cations occupy the tetrahedral sites of lithium layer. Overall, the microstructure of the NCA particle upon charging evolves via a pathway where the intermediate spinel phase is nucleated first, followed by the formation of the spinel domains, and finally the formation of the complete spinel structure.

ASSOCIATED CONTENT

Supporting Information

The Supporting Information is available free of charge on the ACS Publications website at DOI: 10.1021/acs.jpcc.6b10220.

3D/projection views of the second and third structures proposed in Figure 8. CIF files of the three possible structures proposed in Figures 7 and 8 (PDF)
(CIF)
(CIF)
(CIF)

AUTHOR INFORMATION

Corresponding Author

*E-mail: gzhou@binghamton.edu.

DOI: 10.1021/acs.jpcc.6b10220
J. Phys. Chem. C 2017, 121, 1421−1430

ORCID

Hanlei Zhang: 0000-0001-6540-0556

Guangwen Zhou: 0000-0002-9243-293X

Author Contributions

[§]H.Z. and K.K.: These authors contributed equally to this work.

Notes

The authors declare no competing financial interest.

■ ACKNOWLEDGMENTS

This work was supported as part of the NorthEast Center for Chemical Energy Storage (NECCES), an Energy Frontier Research Center funded by the U.S. Department of Energy, Office of Science, Basic Energy Sciences under Award DE-SC0012583. Research was carried out in part at the Center for Functional Nanomaterials, Brookhaven National Laboratory, which is supported by the U.S. Department of Energy, Office of Basic Energy Sciences, under Contract No. DE-AC02-98CH10886. The authors thank Daniel VanHart and In-tae Bae from the Analytical and Diagnostic Lab at Binghamton University for their experimental assistance. We thank John L. Grazul from the Cornell Center for Materials Research (CCMR) at Cornell University for his assistance with TEM sample preparation, under CCMR Grant # NSFDMR1120296.

■ REFERENCES

(1) Whittingham, M. S. Ultimate Limits to Intercalation Reactions for Lithium Batteries. *Chem. Rev.* **2014**, *114*, 11414−11443.

(2) Amin, R.; Ravnsbæk, D. B.; Chiang, Y.-M. Characterization of Electronic and Ionic Transport in $Li_{1-x}Ni_{0.8}Co_{0.15}Al_{0.05}O_2$ (NCA). *J. Electrochem. Soc.* **2015**, *162*, A1163−A1169.

(3) Omar, N.; Bossche, P. V. d.; Coosemans, T.; Mierlo, J. V. Peukert Revisited—Critical Appraisal and Need for Modification for Lithium-Ion Batteries. *Energies* **2013**, *6*, 5625−5641.

(4) Joulié, M.; Laucournet, R.; Billy, E. Hydrometallurgical Process for the Recovery of High Value Metals from Spent Lithium Nickel Cobalt Aluminum Oxide Based Lithium-Ion Batteries. *J. Power Sources* **2014**, *247*, 551−555.

(5) Wei, Z.; Zhang, W.; Wang, F.; Zhang, Q.; Qiu, B.; Han, S.; Xia, Y.; Zhu, Y.; Liu, Z. Eliminating Voltage Decay of Lithium-Rich $Li_{1.14}Mn_{0.54}Ni_{0.14}Co_{0.14}O_2$ Cathodes by Controlling the Electrochemical Process. *Chem. - Eur. J.* **2015**, *21*, 7503−7510.

(6) Reed, J.; Ceder, G.; Van der Ven, A. Layered-to-Spinel Phase Transition in Li_xMnO_2. *Electrochem. Solid-State Lett.* **2001**, *4*, A78.

(7) Albrecht, S.; Kümpers, J.; Kruft, M.; Malcus, S.; Vogler, C.; Wahl, M.; Wohlfahrt-Mehrens, M. Electrochemical and Thermal Behavior of Aluminum-and Magnesium-Doped Spherical Lithium Nickel Cobalt Mixed Oxides $Li_{1-x}(Ni_{1-y-z}Co_yM_z)$ O_2 (M= Al, Mg). *J. Power Sources* **2003**, *119-121*, 178−183.

(8) Boulineau, A.; Croguennec, L.; Delmas, C.; Weill, F. Reinvestigation of Li2mno3 Structure: Electron Diffraction and High Resolution Tem. *Chem. Mater.* **2009**, *21*, 4216−4222.

(9) Lin, F.; Markus, I. M.; Nordlund, D.; Weng, T.-C.; Asta, M. D.; Xin, H. L.; Doeff, M. M., Surface Reconstruction and Chemical Evolution of Stoichiometric Layered Cathode Materials for Lithium-Ion Batteries. *Nat. Commun.* **2014**, *5*.10.1038/ncomms4529

(10) Xiao, L.; Yang, Y.; Zhao, Y.; Ai, X.; Yang, H.; Cao, Y. Enhanced Electrochemical Performance of Submicron Licoo2 Synthesized by Polymer Pyrolysis Method. *J. Solid State Electrochem.* **2008**, *12*, 149−153.

(11) Hwang, S.; Chang, W.; Kim, S. M.; Su, D.; Kim, D. H.; Lee, J. Y.; Chung, K. Y.; Stach, E. A. Investigation of Changes in the Surface Structure of $Li_xNi_{0.8}Co_{0.15}Al_{0.05}O_2$ Cathode Materials Induced by the Initial Charge. *Chem. Mater.* **2014**, *26*, 1084−1092.

(12) Xu, B.; Fell, C. R.; Chi, M.; Meng, Y. S. Identifying Surface Structural Changes in Layered Li-Excess Nickel Manganese Oxides in High Voltage Lithium Ion Batteries: A Joint Experimental and Theoretical Study. *Energy Environ. Sci.* **2011**, *4*, 2223−2233.

(13) Zhang, S.; Xu, K.; Jow, T. Effect of Li_2Co_3-Coating on the Performance of Natural Graphite in Li-Ion Battery. *Electrochem. Commun.* **2003**, *5*, 979−982.

(14) Jung, S. K.; Gwon, H.; Hong, J.; Park, K. Y.; Seo, D. H.; Kim, H.; Hyun, J.; Yang, W.; Kang, K. Understanding the Degradation Mechanisms of $LiNi_{0.5}Co_{0.2}Mn_{0.3}O_2$ Cathode Material in Lithium Ion Batteries. *Adv. Energy Mater.* **2014**, *4*, 1300787.

(15) Hayner, C. M.; Zhao, X.; Kung, H. H. Materials for Rechargeable Lithium-Ion Batteries. *Annu. Rev. Chem. Biomol. Eng.* **2012**, *3*, 445−471.

(16) Tsunashima, K.; Yonekawa, F.; Sugiya, M. Lithium Secondary Batteries Using a Lithium Nickelate-Based Cathode and Phosphonium Ionic Liquid Electrolytes. *Electrochem. Solid-State Lett.* **2009**, *12*, A54−A57.

(17) Kikkawa, J.; Akita, T.; Hosono, E.; Zhou, H.; Kohyama, M. Atomic and Electronic Structures of $Li_{0.44}MnO_2$ Nanowires and Li_2MnO_3 Byproducts in the Formation Process of $LiMn_2O_4$ Nanowires. *J. Phys. Chem. C* **2010**, *114*, 18358−18365.

(18) He, P.; Yu, H.; Li, D.; Zhou, H. Layered Lithium Transition Metal Oxide Cathodes Towards High Energy Lithium-Ion Batteries. *J. Mater. Chem.* **2012**, *22*, 3680−3695.

(19) Ryoo, H.; Bae, H. B.; Kim, Y. M.; Kim, J. G.; Lee, S.; Chung, S. Y. Frenkel-Defect-Mediated Chemical Ordering Transition in a Li−Mn−Ni Spinel Oxide. *Angew. Chem., Int. Ed.* **2015**, *54*, 7963.

(20) Guilmard, M.; Croguennec, L.; Denux, D.; Delmas, C. Thermal Stability of Lithium Nickel Oxide Derivatives. Part I: $Li_xNi_{1.02}O_2$ and $Li_xNi_{0.89}Al_{0.16}O_2$ (x = 0.50 and 0.30). *Chem. Mater.* **2003**, *15*, 4476−4483.

(21) Jalem, R.; Mochiduki, Y.; Nobuhara, K.; Nakayama, M.; Nogami, M. Global Minimum Structure Search in Li_xCoO_2 Composition Using a Hybrid Evolutionary Algorithm. *Phys. Chem. Chem. Phys.* **2012**, *14*, 13095−13100.

(22) Whittingham, M. S. Lithium Batteries and Cathode Materials. *Chem. Rev.* **2004**, *104*, 4271−4302.

(23) Guilmard, M.; Croguennec, L.; Delmas, C. Thermal Stability of Lithium Nickel Oxide Derivatives. Part II: $Li_xNi_{0.70}Co_{0.15}Al_{0.15}O_2$ and $Li_xNi_{0.90}Mn_{0.10}O_2$ (x = 0.50 and 0.30). Comparison with $Li_xNi_{1.02}O_2$ and $Li_xNi_{0.89}Al_{0.16}O_2$. *Chem. Mater.* **2003**, *15*, 4484−4493.

(24) Tarascon, J.-M.; Armand, M. Issues and Challenges Facing Rechargeable Lithium Batteries. *Nature* **2001**, *414*, 359−367.

(25) Arico, A. S.; Bruce, P.; Scrosati, B.; Tarascon, J.-M.; Van Schalkwijk, W. Nanostructured Materials for Advanced Energy Conversion and Storage Devices. *Nat. Mater.* **2005**, *4*, 366−377.

(26) Zheng, J.; Xu, P.; Gu, M.; Xiao, J.; Browning, N. D.; Yan, P.; Wang, C.; Zhang, J.-G. Structural and Chemical Evolution of Li-and Mn-Rich Layered Cathode Material. *Chem. Mater.* **2015**, *27*, 1381−1390.

(27) Thackeray, M. Structural Considerations of Layered and Spinel Lithiated Oxides for Lithium Ion Batteries. *J. Electrochem. Soc.* **1995**, *142*, 2558−2563.

(28) Xiao, J.; Chernova, N. A.; Whittingham, M. S. Layered Mixed Transition Metal Oxide Cathodes with Reduced Cobalt Content for Lithium Ion Batteries. *Chem. Mater.* **2008**, *20*, 7454−7464.

(29) Robert, R.; Villevieille, C.; Novák, P. Enhancement of the High Potential Specific Charge in Layered Electrode Materials for Lithium-Ion Batteries. *J. Mater. Chem. A* **2014**, *2*, 8589−8598.

(30) Bettge, M.; Li, Y.; Gallagher, K. G.; Zhu, Y.; Wu, Q.; Lu, W.; Bloom, I.; Abraham, D. P. Measuring the Impact of Voltage Fade for Selected Li-Intercalating Layered Oxides. *Meeting Abstracts*; The Electrochemical Society, 2013; pp 808−808.

(31) Spiecker, E.; Garbrecht, M.; Jäger, W.; Tillmann, K. Advantages of Aberration Correction for Hrtem Investigation of Complex Layer Compounds. *J. Microsc.* **2010**, *237*, 341−346.

(32) Williams, D. B.; Carter, C. B. *Transmission Electron Microscopy: A Textbook for Materials Science*; Springer: 2009

DOI: 10.1021/acs.jpcc.6b10220
J. Phys. Chem. C 2017, 121, 1421−1430

(33) Buseck, P.; Cowley, J.; Eyring, L. *High-Resolution Transmission Electron Microscopy: And Associated Techniques*; Oxford University Press, 1989.
(34) Lin, F.; Markus, I. M.; Doeff, M. M.; Xin, H. L. Chemical and Structural Stability of Lithium-Ion Battery Electrode Materials under Electron Beam. *Sci. Rep.* **2014**, *4*.10.1038/srep05694
(35) Lu, P.; Yan, P.; Romero, E.; Spoerke, E. D.; Zhang, J.-G.; Wang, C.-M. Observation of Electron-Beam-Induced Phase Evolution Mimicking the Effect of the Charge−Discharge Cycle in Li-Rich Layered Cathode Materials Used for Li Ion Batteries. *Chem. Mater.* **2015**, *27*, 1375−1380.
(36) Ito, A.; Li, D.; Sato, Y.; Arao, M.; Watanabe, M.; Hatano, M.; Horie, H.; Ohsawa, Y. Cyclic Deterioration and Its Improvement for Li-Rich Layered Cathode Material $Li[Ni_{0.17}Li_{0.2}Co_{0.07}Mn_{0.56}]O_2$. *J. Power Sources* **2010**, *195*, 567−573.
(37) Gu, M.; Belharouak, I.; Zheng, J.; Wu, H.; Xiao, J.; Genc, A.; Amine, K.; Thevuthasan, S.; Baer, D. R.; Zhang, J.-G. Formation of the Spinel Phase in the Layered Composite Cathode Used in Li-Ion Batteries. *ACS Nano* **2013**, *7*, 760−767.
(38) Mori, D.; Kobayashi, H.; Shikano, M.; Nitani, H.; Kageyama, H.; Koike, S.; Sakaebe, H.; Tatsumi, K. Bulk and Surface Structure Investigation for the Positive Electrodes of Degraded Lithium-Ion Cell after Storage Test Using X-Ray Absorption near-Edge Structure Measurement. *J. Power Sources* **2009**, *189*, 676−680.
(39) Lee, E.-S.; Manthiram, A. Influence of Doping on the Cation Ordering and Charge−Discharge Behavior of $LiMn_{1.5}Ni_{0.5-x}M_xO_4$ (M= Cr, Fe, Co, and Ga) Spinels between 5.0 and 2.0 V. *J. Mater. Chem. A* **2013**, *1*, 3118−3126.
(40) Thackeray, M. M.; Johnson, C. S.; Vaughey, J. T.; Li, N.; Hackney, S. A. Advances in Manganese-Oxide 'Composite'electrodes for Lithium-Ion Batteries. *J. Mater. Chem.* **2005**, *15*, 2257−2267.
(41) Johnson, C.; Li, N.; Vaughey, J.; Hackney, S.; Thackeray, M. Lithium−Manganese Oxide Electrodes with Layered−Spinel Composite Structures $xLi_2MnO_3 \cdot (1\text{-}x)\ Li_{1+y}Mn_{2-y}O_4$ $(0 < x < 1, 0 \leqslant y \leqslant 0.33)$ for Lithium Batteries. *Electrochem. Commun.* **2005**, *7*, 528−536.
(42) Lee, S.; Yoon, G.; Jeong, M.; Lee, M. J.; Kang, K.; Cho, J. Hierarchical Surface Atomic Structure of a Manganese-Based Spinel Cathode for Lithium-Ion Batteries. *Angew. Chem., Int. Ed.* **2015**, *54*, 1153−1158.
(43) Henke, B.; Davis, J.; Gullikson, E.; Perera, R. A Preliminary Report on X-Ray Photoabsorption Coefficients and Atomic Scattering Factors for 92 Elements in the 10−10,000 Ev Region. *Lawrence Berkeley National Laboratory* **1988**, DOI: 10.2172/919743.
(44) Wang, L.; Maxisch, T.; Ceder, G. A First-Principles Approach to Studying the Thermal Stability of Oxide Cathode Materials. *Chem. Mater.* **2007**, *19*, 543−552.
(45) Mohanty, D.; Sefat, A. S.; Li, J.; Meisner, R. A.; Rondinone, A. J.; Payzant, E. A.; Abraham, D. P.; Wood, D. L., III; Daniel, C. Correlating Cation Ordering and Voltage Fade in a Lithium−Manganese-Rich Lithium-Ion Battery Cathode Oxide: A Joint Magnetic Susceptibility and Tem Study. *Phys. Chem. Chem. Phys.* **2013**, *15*, 19496−19509.
(46) Kim, S.; Ma, X.; Ong, S. P.; Ceder, G. A Comparison of Destabilization Mechanisms of the Layered Na_xMo_2 and Li_xMo_2 Compounds Upon Alkali De-Intercalation. *Phys. Chem. Chem. Phys.* **2012**, *14*, 15571−15578.
(47) Ceder, G.; Van der Ven, A. Phase Diagrams of Lithium Transition Metal Oxides: Investigations from First Principles. *Electrochim. Acta* **1999**, *45*, 131−150.
(48) Key, B.; Bhattacharyya, R.; Morcrette, M.; Seznec, V.; Tarascon, J.-M.; Grey, C. P. Real-Time Nmr Investigations of Structural Changes in Silicon Electrodes for Lithium-Ion Batteries. *J. Am. Chem. Soc.* **2009**, *131*, 9239−9249.
(49) Ricolleau, C.; Denquin, A.; Naka, S. High-Resolution Electron Microscopy Study of Γ-Γt Twin Interfaces in the Lamellar Structure of Tial-Based Alloys. *Philos. Mag. Lett.* **1994**, *69*, 197−204.
(50) Hirahara, K.; Saitoh, K.; Yamasaki, J.; Tanaka, N. Direct Observation of Six-Membered Rings in the Upper and Lower Walls of a Single-Wall Carbon Nanotube by Spherical Aberration-Corrected Hrtem. *Nano Lett.* **2006**, *6*, 1778−1783.

DOI: 10.1021/acs.jpcc.6b10220
J. Phys. Chem. C 2017, 121, 1421−1430